F. Giussani, A. Montorfano, F. Piscaglia, A. Onorati, J. Elie, S.M. Aithal
Dynamic VOF Modelling of the Internal Flow in GDI Fuel Injectors
Energy Procedia, Vol. 101, 2016, p. 574-581
doi:10.1016/j.egypro.2016.11.073

Available online at www.sciencedirect.com

ScienceDirect

Energy Procedia 101 (2016) 574 – 581

Energy Procedia

71st Conference of the Italian Thermal Machines Engineering Association, ATI2016,
14-16 September 2016, Turin, Italy

Dynamic VOF modelling of the internal flow in GDI fuel injectors

F. Giussani[a,*], A. Montorfano[a], F. Piscaglia[a], A. Onorati[a], J. Hélie[b], S. M. Aithal[c]

[a]*Dip. di Energia, Politecnico di Milano, via Lambruschini 4, I-20156 Milan (Italy)*
[b]*Continental Automotive SAS, 1 av. Paul Ourliac BP 1149, 31036 Toulouse Cedex 1 (France)*
[c]*Argonne National Laboratory, 9700 S. Cass Avenue, Argonne, IL 60439 (USA)*

Abstract

High-fidelity transient simulations of turbulent flows usually require highly resolved grids, leading to unacceptable large computational wall times even on large supercomputers. In an attempt to address this limitation, a hybrid Large-Eddy/Reynolds-Averaged scale-adaptive turbulence model has been applied together with a Volume-Of-Fluid (VOF) solver in OpenFOAM to simulate cavitation in the injector nozzle and primary fuel atomization during the opening event of a GDI gasoline-injector for automotive applications. A dynamic mesh strategy based on topological changing grids has been used to handle the moving geometry. In addition, algorithmic developments are presented to improve parallel performance on modern supercomputers. The outcome of the scalability tests are reported together with results from simulations on the Continental XL3.0 6-hole injector performed at the Argonne National Laboratory.

Peer-review under responsibility of the Scientific Committee of ATI 2016.

Keywords: Hybrid RANS/LES, scale-resolving turbulence modeling, VOF, GDI injectors, Dynamic Mesh, Cavitation, Topological Changes, OpenFOAM

1. Introduction

Turbulence certainly has a direct impact on thermodynamic efficiency, brake power and emissions of the engine, since its influence extends from volumetric efficiency to air/fuel mixing, combustion and heat transfer. In a gasoline engine, there are two strategies for injecting the fuel: Port Fuel Injection (PFI), a well known technology to favor air/fuel mixing, and Gasoline Direct Injection (GDI), which consists in injecting the fuel directly into the cylinder. GDI is becoming a common solution in automotive industry since it allows for a great flexibility in the air/fuel ratio, leading to low fuel consumption and emissions at light loads (lean or stratified mode) and high power output during rapid accelerations and heavy loads (power mode). These different conditions are not only related to the amount of fuel injected into the combustion chamber, but also to the way injection is performed: level of atomization, penetration and diffusion of fuel. Experimental campaigns showed that spray formation is mainly influenced by the geometry of the injector itself (L/D ratio, number of holes, internal geometry), operating pressure and needle lift curve. Fuel is characterized by high velocities (order of hundreds of meters per second) and reduced timescales, so that time-transient phenomena and compressibility play an important role. Moreover, because of the strong acceleration of the liquid phase inside the injector nozzle, pressure may drop below the saturation value causing the onset of cavitation, which strongly modifies the internal flow field due to the presence of bubbles. Thus a better comprehension of spray characteristics could help to improve engine performance and injector design. Simulating the injector opening event and the spray primary breakup are still on the frontier of modern modeling science. Since primary breakup is strictly related to turbulence inside the injector, a correct way to describe turbulence is crucial for a successful simulation. In this sense, a time-resolved approach (Large Eddy Simulation, LES) seems the most appropriate to model turbulence in injectors and also a straight-forward way to overcome the intrinsic lack of resolution in time of the Unsteady Reynolds-Averaged Navier-Stokes (URANS) equations. On the other hand, LES requires extremely high grid resolution, in particular near the high-speed flow regions and near the walls. A scale resolving approach represents a very promising way to overcome the above mentioned

*Tel.:+39 02 2399 3909; fax:+39 02 2399 3913. E-mail address:filippo.giussani@polimi.it

Peer-review under responsibility of the Scientific Committee of ATI 2016.
doi:10.1016/j.egypro.2016.11.073

limitations, since it combines the best features of RANS (to model the jet-core and to model near-wall turbulence) and LES where possible; as a result, it is possible to solve the largest turbulent scales and thus capture the typical ligament structures of primary breakup and vortex cavitation inside the nozzle in a reasonable amount of computational time. In this work, a scale-adaptive turbulence model called DLRM (Dynamic Length Resolution Model) has been used [1]; the model belongs to the family of the hybrid models, since it automatically switch between LES and URANS according to the local mesh resolution and time-step advancement [1]. Finally, part of the paper address issues with spray modeling. Disperse sprays are usually simulated by a Lagrangian/Eulerian approach [2]: particles reside in the Eulerian grid cells and introduce source terms in the Eulerian conservation laws to account for interactions between the two phases. To simulate fuel injection, the continuous liquid core in the near-nozzle region is modeled by discrete parcels which typically are assumed to have the same characteristic size as the nozzle exit diameter and phenomenological models are used to account for breakup [3], as well as collision and coalescence of liquid droplets [4]. The above mentioned method requires a precursor nozzle flow simulation of the Eulerian liquid phase to predict the flow conditions at the nozzle exit [5]. The coupling between the internal and the external nozzle simulation is inherently weak, due to potential inconsistencies of the two-phase models in the two separate simulations. In theory, engine sprays and sprays in general could be better described using a continuum for both the liquid and the gas phases, where conservation laws are solved under Eulerian flow assumptions and grid is refined until grid resolution allows for solving droplets or bubbles without introducing any conceptual particles. In such a case, a transport equation for an indicator function, e.g., a "level-set" function or the volume fraction, on which the Volume-Of-Fluid (VOF) approach is based, is used to track the liquid-gas interface [6, 7, 8]. Also, since pressure inside the injector nozzle may drop below saturation pressure, a source term for cavitation in the momentum equation of the transported phases has been included. Moreover, a mesh motion strategy based on topological changes [9, 10, 11] has been coupled with the VOF solver and applied to simulate the needle movement: the aim was to study the early stage of the cavitating flow in the internal nozzle at the injector opening, where the continuum hypothesis is assumed to be valid. The developed code in the OpenFOAM technology has been tested on large supercomputers at the Argonne National Laboratory. New algorithms to perform load balanced constrained domain decomposition, compatible with topological changes, to enable strong scalability of the solver, have been developed.

2. Test case

The selected test case chosen for validation and testing of the dynamic VOF solver is a 6-hole injector prototype Continental XL3.0 (Fig. 1, left), especially developed for investigations in the framework of the collaborative project FUI MAGIE. Measured experimental needle lift data (Fig. 1, right) were performed by Dr. Jin Wang at Argonne National Laboratory.

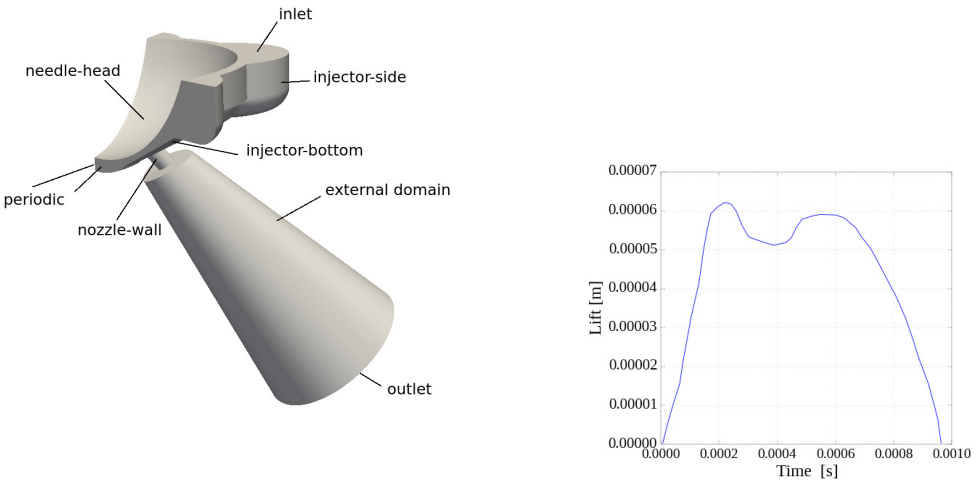

Fig. 1: XL3.0 6-hole injector; only 1/6 of the real component has been simulated (left). Injector needle lift after start of injection (right).

In the experiments, conditions of liquid gasoline were $T = 20°C$ and $p = 30$ bar. Fuel was injected at ambient temperature in a large transparent chamber filled with air at ambient pressure. When the static pressure inside the nozzle drops below the vaporization pressure of the fuel, the liquid starts to cavitate and turns into the gaseous state of the fuel. Under these conditions, three phases of the fluid are observed: air, fuel vapor and liquid.

3. Two-phase VOF solver and cavitation model

A two-phase dynamic (isothermal and immiscible) VOF incompressible solver, including a cavitation model, has been used to simulate the injector opening event; in the simulations the liquid is assumed to be injected into a plenum chamber. Even if in the real experiments three phases of the fluid coexist (air, fuel vapor and liquid fuel), the problem has been simplified by considering only the liquid and vapor state of the fuel, both behaving as incompressible fluids: this is consistent with the real physics of the problem, since in early fuel injection (which is the object of the present study) the fuel vapor does not reach the cavitating region in the nozzle and the effect of the gas/liquid interface compression does not have a significant effect. This assumption would not be valid if late injection is simulated. The dynamic VOF solver includes a transport equation for the liquid fraction α_l (Eq. (1)), that is defined as the ratio of the liquid volume contained in a cell to the total liquid volume. The conservation equation for α_l is:

$$\frac{\partial \alpha_l}{\partial t} + \nabla \cdot (\alpha_l(\mathbf{U} - \mathbf{U}_b)) + \nabla \cdot [\alpha_l(1-\alpha_l)\mathbf{U}_c] = \frac{\dot{m}}{\rho_l} \tag{1}$$

where $\dot{m}$ is the mass source due to cavitation and $(\mathbf{U} - \mathbf{U}_b)$ is the relative velocity field between the fluid and the moving boundary. From the definition of α, it results that $\alpha_l + \alpha_v = 1$ where subscripts l and v stand for liquid and vapor respectively. The volume fraction is used to scale the physical properties of the mixture as:

$$\rho = \rho_l\alpha_l + (1-\alpha_l)\rho_v \text{ and } \mu = \mu_l\alpha_l + (1-\alpha_l)\mu_v \tag{2}$$

The weighted physical properties of mixture are then used in the momentum equation:

$$\frac{\partial(\rho\mathbf{U})}{\partial t} + \nabla \cdot (\rho(\mathbf{U} - \mathbf{U}_b)\mathbf{U}) - \nabla \cdot \mu\nabla\mathbf{U} - \rho\mathbf{g} = -\nabla p - \mathbf{F}_s \tag{3}$$

where $\mathbf{F}_s$ is surface force defined as $\sigma\kappa(x)\mathbf{n}$ with curvature $\kappa(x) = \nabla \cdot \mathbf{n}$, interface normal face unit vector $\mathbf{n} = \nabla\alpha_l/|\nabla\alpha_l|$, and surface tension σ. The last term on the left-hand side of Eq. 1 is known as the artificial compression term and it is non-zero only at the interface due to $\alpha_l(1-\alpha_l)$. The compression term has the role of shrinking the phase-interface towards a sharper one [12]. The compression term does not bias the solution in any way and it only corrects the flux of α_l in the interface-normal direction. In order to enforce this procedure, Weller [13] suggested the compression velocity to be calculated as:

$$\mathbf{U}_c = C_\alpha|\mathbf{U}|\mathbf{n} \tag{4}$$

The intensity of the interface compression is controlled by a constant C_α, which yields no compression when zero, a conservative compression for $C_\alpha = 1$ and high compression for $C_\alpha > 1$ [12]. On the right-hand side, the mass source for cavitation is modeled according to the theory by Schnerr and Sauer [14]. According to it, there are several vapor bubbles, also called nuclei, inside the liquid that act as the initial sources of the phase change; cavitation starts from their locations and due to their presence. The mass transfer rate between liquid and vapor phases can be defined as follows:

$$\dot{m} = \alpha_l\dot{m}_{\alpha v} + (1-\alpha_l)\dot{m}_{\alpha c} \tag{5}$$

where:

$$\dot{m}_{\alpha c} = C_c\alpha_l\frac{3\rho_v\rho_l}{R_b\rho}\sqrt{\frac{2}{3\rho_l|p-p_{sat}|}} \cdot \max(p-p_{sat}, 0) \tag{6}$$

$$\dot{m}_{\alpha v} = C_v(1+\alpha_n-\alpha_l)\frac{3\rho_v\rho_l}{R_b\rho} \cdot \sqrt{\frac{2}{3\rho_l|p-p_{sat}|}}\min(p-p_{sat}, 0) \tag{7}$$

with C_c and C_v as, respectively, the condensation and vaporization rate coefficients chosen by the user. These coefficients represent the relaxation time that either vapor or liquid phase needs to be transferred into the other phase. According to previous works [15] C_v and C_c are chosen equal to 1, that equals to consider the same behavior for condensation and vaporization rate. Moreover the reciprocal bubble radius is defined as:

$$\frac{1}{R_b} = \left[\frac{4}{3}\frac{\pi n\alpha_l}{(1+\alpha_n-\alpha_l)}\right]^{1/3} \tag{8}$$

$\alpha_n = V_n/1 + V_n$ is the nuclei volume fraction; the latter is computed as:

$$V_n = \frac{n\pi {d_n}^3}{6} \tag{9}$$

with n as the number of nuclei per unit volume and d_n their diameter. Since at the moment there are no experiments about nucleation characteristics of fuels, size and distribution of nuclei can be taken from experiments carried out with water. In this

work, it is assumed a uniform nuclei distribution of $n = 1.6 \cdot 10^{-8}$ m^{-3} with a diameter $d_n = 2$nm. Moreover, depending on the local properties of the flow, the extra diagonal terms in the linear system matrix of Eq. (1) can become very large (due to very high phase change rate), thus impairing the convergence rate. In order to improve the solution stability, the source term needs to be rewritten, so that Eq. 1 is formulated by decomposing the volume source $\dot{V}$ in an implicit and an explicit part:

$$\dot{V} = \left[\frac{1}{\rho_l} - \alpha_l\left(\frac{1}{\rho_l} - \frac{1}{\rho_v}\right)\right]\dot{m} = A_\alpha \dot{m} = A_\alpha(\dot{m}_{\alpha v} - \dot{m}_{\alpha c})\alpha_l + A_\alpha \dot{m}_{\alpha c} = (\dot{V}_v - \dot{V}_c)\alpha_l + \dot{V}_c \tag{10}$$

the former being $(\dot{V}_v - \dot{V}_c)$, which enters the system matrix as a diagonal coefficient; on the other hand, the explicit part of the source term $\dot{V}_c$ will be written on the right-hand side of the linear system. The final form of the conservation equation of α_l (Eq. (11)) therefore reads:

$$\frac{\partial \alpha_l}{\partial t} + \nabla \cdot (\alpha_l(\mathbf{U} - \mathbf{U}_b)) + \nabla \cdot [\alpha_l(1 - \alpha_l)\mathbf{U}_c] = (\dot{V}_v - \dot{V}_c)\alpha_l + \dot{V}_c \tag{11}$$

4. Dynamic mesh handling and parallel optimization

The moving mesh functionality used in this work is described in [9, 10] and it has been applied as described in [11]. The injector opening event is simulated by dynamically attaching and detaching the conformal interface represented by the set of faces `detachFaces` in Fig. 2a, while a prescribed vertical motion is set for the boundary `needleHead` and for the corresponding moving cell set. Initially the first layer cell attached to `bottomFaces` and `topFaces` are respectively stretched and shrunk. Due to the very small gap between the injector needle and the injector body at closure ($O(\delta) = 10\,\mu$m), the mesh handling could look particularly difficult: cell sizes change by orders of magnitude and this can impair the mesh smoothness in the near-nozzle region. To overcome this issue, when cell layers reach the max/min layer thickness specified by the user, automatic addition/removal is triggered, ensuring constant cell quality during the whole simulation.

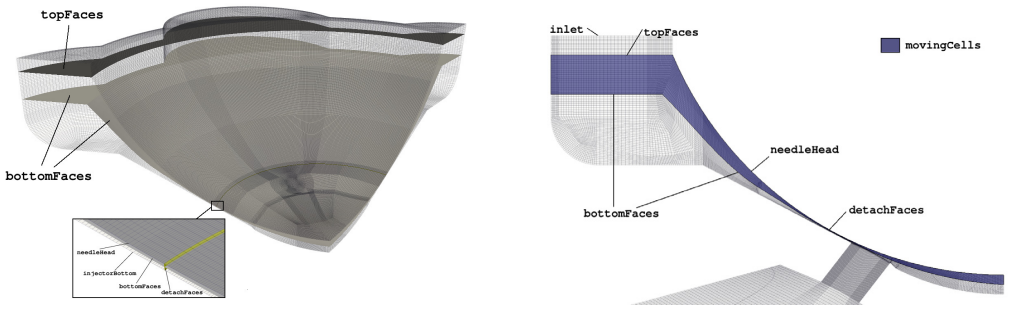

(a) (b)

Fig. 2: (a) Detail of the face sets used to perform dynamic layering: `topFaces` and `bottomfaces` are used to perform layer addition removal, while `detachFaces` are used to perform dynamic attach/detach; `needle-head` is the needle patch where boundary condition of `movingWallVelocity` has been applied. (b) Cell sets used for decomposition

To run parallel simulations, the Finite Volume (FV) mesh has to be decomposed into a set of subdomains, each to be assigned to a single core for processing. In simulations involving mesh motion with topological changes, new constraints in domain decomposition arise. In OpenFOAM®, as well as in most of the CFD codes, topological changes cannot occur across inter-processor patches between neighboring subdomains and the decomposition algorithm must be constrained in this sense. In other words, in regions where layer Addition/Removal (A/R) occurs, inter-processor faces cannot be parallel to layer A/R surface as shown in Fig. 2b. Nevertheless, it is important for the decomposition to remain balanced despite the aforementioned restrictions; in addition, the algorithm should require minimal user intervention, allowing the automation of case setup for large simulation campaigns. A new strategy for mesh decomposition, which considers all the aforementioned aspects, has been developed and applied to the GDI injector. The decomposition algorithm proceeds as follows:

1. The grid is divided into several regions, in accordance with the decomposition constraints (layer A/R zones, attach/detach zones, static parts Fig. 2b). Each mesh region is decomposed into a number of subdomains, depending on the size of the region;
2. All the face sets where dynamic layering is triggered (e.g. `bottomFaces`) are decomposed and subsets of faces are distributed among processors. For specified cell sets, cell decomposition is propagated perpendicularly to the face set using a cell-face walk algorithm, over the entire mesh region where layer addition/removal can be triggered, as shown in Figs. 3a-3b;

3. The remaining cells of the mesh are distributed among processors using non-constrained decomposition Fig. 3c

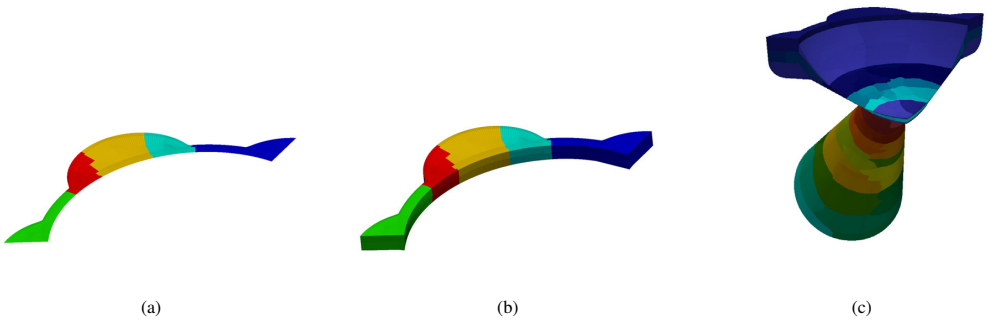

(a) (b) (c)

Fig. 3: Overview of decomposition strategy: (a) Decomposition of face set `topfaces` using Scotch method; (b) Propagation of face set decomposition tho whole cellSet; (c) Complete decomposition

The decomposition strategy outlined above is very flexible, allowing for an almost perfect cell distribution (load balancing) over the processors with complex geometries and topological changes. The domain decomposition and overall balancing of the mesh used in this work is shown in Fig. 4. For similar geometries, the steps for domain decomposition can be easily automated, thus enabling automatic case setup in optimization/validation campaigns.

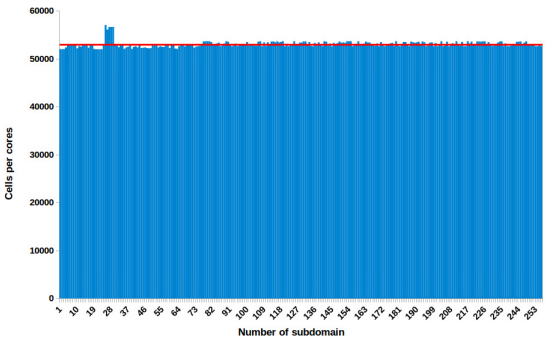

Fig. 4: Histogram of number of cells per core. Red line represents mean value

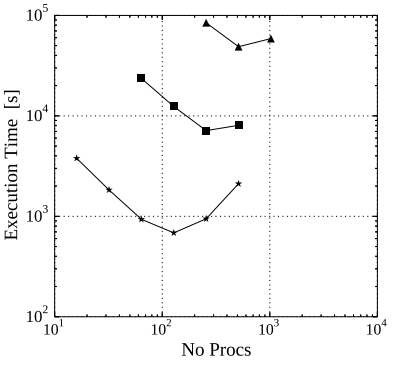

Fig. 5: Left: Wallclock time vs number of subdomains. Right: Wallclock time vs cells per processor. –★– 1M mesh, –■– 8M mesh , –▲– 64M mesh. Simulation time is 0.05 s for 1M and 8M cases, 0.025 s for 64M case.

Scalability tests were performed with the same solver on a simplified test case. Results are shown in Fig. 5. Three meshes with progressive refinement were tested, i.e., with 1M, 8M, and 64M cells. Speedup is linear at least for a certain number of subdomains per each mesh. The reason for the degradation of parallel performance over a certain threshold is still under investigation. However, since the present case has a number of cells that is very similar to one mesh used in the test (respectively 11M cells vs. 8M cells), a decomposition over 256 subdomains has been chosen. Moreover, the same tests [16, 17] proved that using Preconditioned Conjugate Gradient (PCG) method instead of Geometric-Algebraic Multi-Grid (GAMG) to solve Poisson equation for pressure, can reduce the overall wall clock time but does not affect the scalability behavior, especially when a large amount of cores are used. On the other hand, there is also a chance that the performance decay is caused by a different convergence behavior of some subdomains rather than an increased communication overhead. In case the interface-tracking resolution is delegated only to a few processors out of many, the consequent increased difficulty in solving the Poisson Equation (because of sharp pressure and density changes across the liquid/gas interface) on those few subdomains can act as a bottleneck on the overall clock time. As a consequence, the parallel performance of the run might be impaired.

5. Case Setup

Geometry. The injection chamber has been approximated by a conical volume, to limit the overall number of cells while preserving the walls sufficiently far to interfere with the internal flow. Moreover, from previous work of Lu [15], it has been

seen that such geometry approximation coupled with non-reflecting outlet condition [18] does not influence break-up phenomena. The block-structured, fully hexahedral FV mesh had 12M cells at injector closure. The approach chosen for turbulence modeling allows for the use of an increased cell size in the external region, where velocities are lower and turbulence dynamics is less critical for the global solution, limiting the overall number of cells. On the other hand, where cavitation occurs and a large amount of turbulence is generated, highly-resolved meshes are required to accurately capture the physics. Because of the Courant-Friedrichs-Lewy (CFL) criterion, this greatly limits the size of time steps. n-Heptane has been chosen as fluid since its properties approximate the behavior of gasoline quite well.

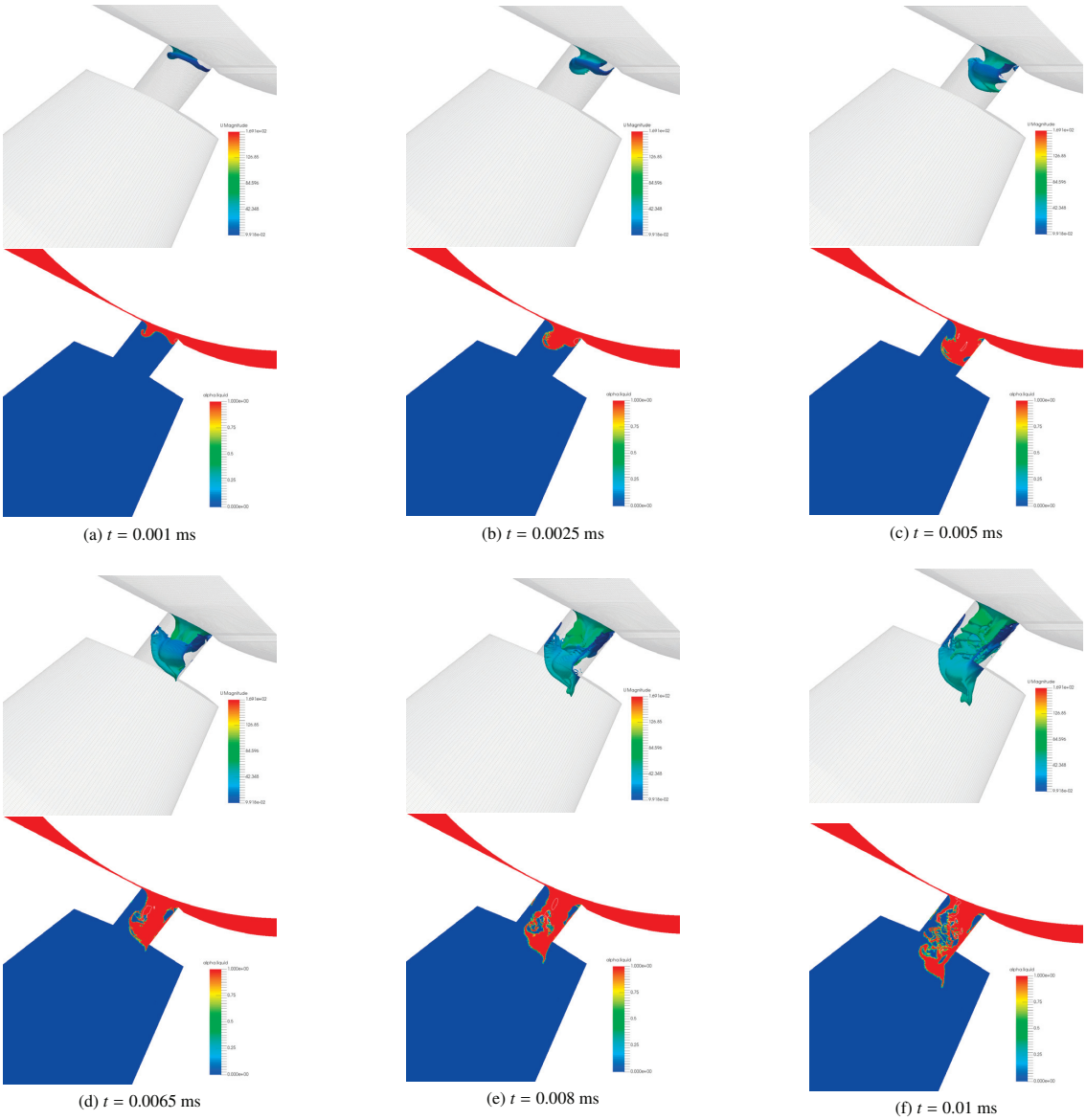

(a) t = 0.001 ms (b) t = 0.0025 ms (c) t = 0.005 ms

(d) t = 0.0065 ms (e) t = 0.008 ms (f) t = 0.01 ms

Fig. 6: Sequence of snapshots of the spray exiting the nozzle following SOI. Top row: isosurface with $\alpha_l = 0.5$, bottom row: sliced view of the above, with constant pressure line at $p = p_{sat}$.

Numerical setup. Second-order backward Euler scheme for temporal discretization has been applied in the simulations. Extensive development has been done to preserve second order temporal accuracy with dynamic addition of cell layers in

OpenFOAM [11, 19]. Pressure-velocity coupling is achieved by means of a transient-SIMPLE algorithm. The phase-fraction equation (Eq. (1)) is solved explicitly at the beginning of each time iteration by means of the Multi Universal Limiter for Explicit Solution (MULES) [20], a Flux Corrected Transport method developed by Weller to ensure boundedness of the α flux on all faces. In addition, special Total Variation Diminishing (TVD) methods are used for compression velocity term $\nabla\cdot[\alpha_l(1-\alpha_l)\mathbf{U}_c]$ and $\nabla\cdot(\mathbf{U}\alpha_l)$. The former has been discretized with `interfaceCompression` scheme, the latter with `vanLeer`, as suggested by Weller [13]. For convective term $\nabla\cdot(\phi\mathbf{U})$ a Linear Upwind with Stabilized Transport (LUST) scheme has been selected, while pure second order spatial discretization has been used for divergence term of turbulent variables. The hybrid RANS/LES Dynamic Length-scale Resolution Model (DLRM) by Piscaglia *et al.* [21] has been chosen for this simulation. Due to the strong unsteady character of the flow and the importance of wave acoustics in the evolution of the flow field, the maximum CFL of the has been set to 1. The Length-Scale Resolution parameter – which is used by DLRM to discriminate between resolvable and unresolvable length scales – has been set to 5.

6. Injector opening: preliminary results

Since the simulation is very demanding in terms of computational resources, only partial results are available at the time this paper is written. Fig. 6 show the evolution of n-Heptane spray inside the combustion chamber up to 0.01 ms After Start Of Injection (ASOI). As the needle starts opening, the nozzle is filled progressively with a non uniform distribution of liquid due to the high level of turbulence; therefore, the tip of the spray jet does not have the typical mushroom shape described by other authors [15, 22], who analyzed the primary breakup at fixed needle position (maximum lift). On the other hand, the jet tip presents a symmetrical shape probably caused by the counter-rotating vortices that usually forms in the nozzle. By looking at the constant pressure line at $p = p_{sat}$, the main cavitation region is detected in correspondence of the *vena contracta* between the needle sac and the nozzle entry. A recirculation vortex is formed in this point, where pressure drops below the saturation value. The pocket of vapor is then transported towards the jet core and it is disrupted by the turbulent structures that reside there. A clearer idea of the turbulent structures that are formed in the nozzle can be observed in Fig. 7. Similarly to [15], a pair of counter-rotating vortices, roughly aligned with the nozzle axis, is formed in the jet core together with finer turbulent structures responsible of the instability of the jet (Fig. 7). As the recirculation region formed in regions corresponding to the vena contracta, the counter-rotating vortices could also be responsible for cavitation. Finally, the incipient primary breakup can also be observed at such an early stage of the injection: in Fig. 6, the development of some unstable structures like the instability wave on the upper side of the jet and the wrinkling of the liquid front as it enters the injection chamber can be observed.

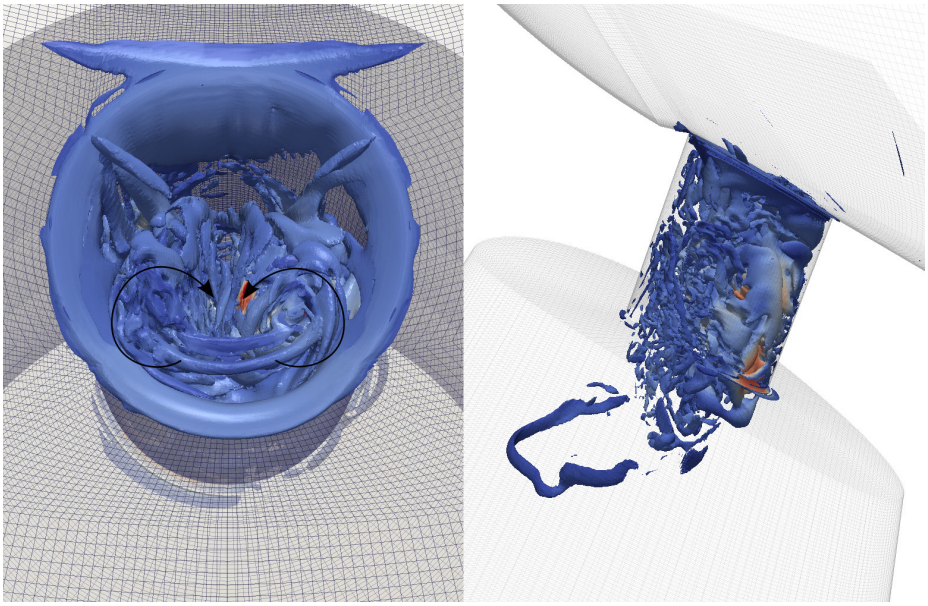

Fig. 7: Vortical structures inside nozzle from at time $9.5 \cdot 10^{-6}$ s (Q criterion). Upper view (left), side view (right).

7. Conclusions

The paper shows current developments done on dynamic simulation of multiphase flows of GDI injectors, with particular focus on the coupling of an incompressible two-phase VOF solver with the cavitation model in a framework where the dynamic mesh based on topological changes and automatically handled in parallel. The solver has been applied to the simulation of a gasoline injector specifically designed for GDI engines and provided by Continental Automotive SAS. The case has been set up to simulate the early stages of the gasoline injection, using topological changes to implement both mesh motion and injector. Detailed features of the flow structures during the primary breakup are detected, which are fully in accordance with the findings of [15]; in this sense, the approach can be considered as reliable and therefore it can be applied during the design phase to study the influence of the injector geometry on flow cavitation. The solver also proved to be very stable: boundedness of the liquid fraction α_l was always preserved during the simulations even in presence of topological changes, so the method can be assumed to be fully conservative. Also, second-order accuracy was preserved both in space and time, which is not trivial in presence of dynamic topologically changing grids. Finally, a new decomposition method to enable good scalability of the code on large supercomputers have been developed. The developed code presented in this paper uses the OpenFOAM version released by the OpenFOAM® Foundation as a common code base.

8. Acknowledgments

Authors would like to kindly thank LCRC (Laboratory Computing Resource Center), Argonne National Lab, for making available the computing resources through the HPC cluster Blues within the PETSc-Foam project.

[1] F. Piscaglia, A. Montorfano, A. Onorati, Scale adaptive filtering technique for turbulence modeling of unsteady flows in IC engines, SAE Int. J. Engines, Paper n. 2015-01-0395, 2015Http://dx.doi.org/10.4271/2015-01-0395.

[2] K. John, Dukowicz, A particle-fluid numerical model for liquid sprays, Journal of Computational Physics 35 (2) (1980) 229–253. doi:http://dx.doi.org/10.1016/0021-9991(80)90087-X.
URL http://www.sciencedirect.com/science/article/pii/002199918090087X

[3] Reitz, D. Rolf, Modeling atomization processes in high-pressure vaporizing sprays, Atomization and Spray technology 3 (4) (1987) 309–337.

[4] A. Amsden, A block-structured program for engines with vertical and canted valves.

[5] E. Giannadakis, M. Gavaises, C. Arcoumanis, Modeling of cavitation in Diesel injector nozzles, International Journal of Fluid Mechanics 616 (2008) 153–193. doi:http://dx.doi.org/10.1017/S0022112008003777.

[6] T. Menard, S. Tanguy, A. Berlemont, Coupling level set/VOF/ghost fluid methods: Validation and application to 3D simulation of the primary break-up of a liquid jet, International Journal of Multiphase Flow 33 (5) (2007) 510 – 524. doi:http://dx.doi.org/10.1016/j.ijmultiphaseflow.2006.11.001.
URL http://www.sciencedirect.com/science/article/pii/S0301932206001832

[7] H. Pitsch, O. Desjardins, Deatailed umerical investigation of turbulent atomization of liquid jets, Atomization and Sprays 20 (4) (2010) 311–336.

[8] S. S. Deshpande, M. F. Trujillo, X. Wu, G. Chahine, Computational and experimental characterization of a liquid jet plunging into a quiescent pool at shallow inclination, International Journal of Heat and Fluid Flow 34 (0) (2012) 1 – 14. doi:http://dx.doi.org/10.1016/j.ijheatfluidflow.2012.01.011.
URL http://www.sciencedirect.com/science/article/pii/S0142727X12000197

[9] F. Piscaglia, A. Montorfano, A. Onorati, An extension of the dynamic mesh handling with topological changes for LES of ICE in OpenFOAM, SAE paper 2015-01-0384, 2015, SAE World Congress Exhibition, Detroit, Michigan (USA)Http://dx.doi.org/10.4271/2015-01-0384.

[10] F. Piscaglia, A. Montorfano, A. Onorati, Development of Fully-Automatic Parallel Algorithms for Mesh Handling in the OpenFOAM-2.2.x Technology, SAE Technical Paper 2013-24-0027http://dx.doi.org/10.4271/2013-24-0027.

[11] F. Piscaglia, A. Montorfano, et al., Hybrid RANS/LES of Moving Boundary Problems: Application to Cavitating Sprays and In-Cylinder Flows, in: International Multidimensional Engine Modeling User's Group Meeting At the SAE Congress, 2016, https://imem.cray.com/agenda.html.

[12] E. Berberovic, Investigation of free-surface flow associated with drop impact: Numerical simulations and theoretical modeling, Ph.D. thesis, Technische Universität, Darmstadt (November 2010).
URL http://tuprints.ulb.tu-darmstadt.de/2319/

[13] H. Weller, A new approach to vof-based interface capturing methods for incompressible and compressible flow, Technical report tr/hgw/04,opencfd ltd., Technical Report TR/HGW/04,OpenCFD Ltd. (2008).

[14] G. Schnerr, J. Sauer, Unsteady cavitating flow – a new cavitation model based on a modified front capturing method and bubble dynamics., ASME Fluids Engineering Summer Meeting, June 2011-15, Boston (USA).

[15] N. Lu, F.-X. Demoulin, J. Reveillon, J. Chesnel, Large eddy simulation of cavitation and atomization in injector flows using openfoam, ILASS – Europe 2014, 26th Annual Conference on Liquid Atomization and Spray Systems, Bremen, Germany.

[16] J. Hélie, J. Chesnel, N. LU, Parallel performance of OpenFOAM in industrial applications, Tech. rep., PRACE project pa1507 (2015).

[17] A. Montorfano, F. Giussani, F. Piscaglia, J. Hélie, Parallel performance of OpenFOAM in industrial applications, Tech. rep., PRACE project pa3053 (2016).

[18] F. Piscaglia, A. Montorfano, A. Onorati, Development of a Non-Reflecting Boundary Condition for Multidimensional Nonlinear Duct Acoustic Computation, Journal of Sound and Vibration 332 (4) (2013) 922–935.

[19] F. Piscaglia, "Ongoing and future perspective developments in OpenFOAM", Keynote invited talk at the 4th Annual ESI-OpenCFD OpenFOAM User Conference 2016, Cologne (Germany).

[20] The OpenFOAM Foundation, Free open-source CFD, http://www.openfoam.org.

[21] F. Piscaglia, A. Montorfano, A. Onorati, A Scale Adaptive Filtering Technique for Turbulence Modeling of Unsteady Flows in IC Engines, SAE Int. J. Engines, Paper n. 2015-01-0395http://dx.doi.org/10.4271/2015-01-0395.

[22] G. Stiesch, Modeling Engine Spray and Combustion Processes, Heat and Mass Transfer, Springer Berlin Heidelberg, 2003.
URL https://books.google.co.uk/books?id=4A35ABlw1wgC